plasma

MDPI

Article

Methylene Blue Degradation Using Non-Thermal Plasma

Hae Kwang Kim [1,2], Geon Woo Yang [1] and Yong Cheol Hong [1,3,*]

[1] Institute of Plasma Technology, 37 Dongjansan-ro, Gunsan 54004, Republic of Korea
[2] Department of Mechanical Engineering, Chungbuk National University, 1, Chungdae-ro, Seowon-gu, Cheongju-si 28644, Republic of Korea
[3] KFE-School, University of Science and Technology (UST), 217, Gajeong-ro, Yuseong-gu, Deajeon 34113, Republic of Korea
* Correspondence: ychong@kfe.re.kr

Abstract: Methylene blue ($C_{16}H_{18}ClN_3$) dye can be decomposed using non-thermal plasma. However, there is a problem in that the maintenance of electrodes and dielectrics is necessary due to the durability and heat generation problems due to the high temperatures. Therefore, in this study, a comparative experiment was performed between the flat DBD plasma module and the diffuser DBD module under the same conditions. For methylene blue decomposition, the characteristic changes in the air flow rate, ozone production rate, energy consumption rate, and decomposition rate were compared. In the experiment, 7 L water was placed in a 15 L reactor, and measurements were performed for approximately 1 h. We performed the same process by setting the initial methylene blue concentration to 143 mg/L. According to the results, the flat DBD module achieved a decomposition rate of 100% in 40 min, an energy yield of 46.7 g/kWh, and an ozone generation amount of 6.5 g/h. The diffuser DBD module achieved a decomposition rate of 90%, an energy production of 24.6 g/kWh, and an ozone generation of 1.97 g/h in 60 min.

Keywords: dielectric barrier discharge; methylene blue; plasma; oxidative degradation; diffuser

Citation: Kim, H.K.; Yang, G.W.; Hong, Y.C. Methylene Blue Degradation Using Non-Thermal Plasma. *Plasma* **2024**, *7*, 767–779. https://doi.org/10.3390/plasma7030040

Academic Editors: Carles Corbella and Andrey Starikovskiy

Received: 4 July 2024
Revised: 12 September 2024
Accepted: 14 September 2024
Published: 19 September 2024

1. Introduction

With the development of the dyeing industry, the use of synthetic dyes has increased, which has led to serious environmental and health problems due to the discharge of these dyes into industrial wastewater [1]. More than 7105 tons of dyes are produced annually, increasing research on pollutant removal [2–4]. Due to the complex structure of the auxiliary pigments (water-soluble binding compounds) and chromophores in organic dye molecules, the removal of dye is generally difficult [5,6] and the use of hydroxyl radicals generated during the advanced oxidation process (AOP) is insufficient [7,8]. Therefore, alternative removal methods are necessary. A representative technology involves the use of low-temperature plasma to remove organic substances through oxidation by reactive oxygen species (ROS) such as ·OH, ·O, O_3, H_2O_2 and reactive nitrogen species, which can be converted into small molecules, making them effective for dye treatment [9].

Additionally, this process does not require additional chemicals and removes contaminants at atmospheric pressure [10]. The flat dielectric barrier discharge (DBD) and diffuser DBD introduced herein are compact technologies that are inexpensive to manufacture and produce high concentrations of ozone. Because air is used as the discharge gas, such technology is also advantageous in terms of the operating costs. The most important reactions for ROS generation in such systems are as follows:

$$O_2 + e \rightarrow O + O + e \quad (1)$$

$$O + H_2O \rightarrow 2OH \quad (2)$$

$$\cdot OH + \cdot OH \rightarrow H_2O_2 \quad (3)$$

$$O + O_2 \rightarrow O_3 \quad (4)$$

A high-energy electron typically leads to the dissociation of O_2 in air and the formed atomic oxygen can then induce the continuous formation of H_2O_2 and O_3. The reactions used in the experiment take place in a gas/liquid interface.

Flat DBD plasma reactors have attracted increasing attention because they offer high energy efficiency for treating contaminants in water [11]. Additionally, a large amount of ozone can be generated from the atmosphere and injected into the reactor, and high-density plasma-activated species can be produced without high energy consumption [12]. The gas discharged by non-thermal plasma (NTP) is sent to the discharge area, and plasma is generated and dispersed into a liquid phase by porous ceramics. This process can improve the decomposition efficiency of pollutants by increasing the mass transfer efficiency of active species into the liquid.

However, the active species used to remove dyes are mostly ozone. Most active species have short lifespans and disappear during the diffusion process [13–18], which increases the difficulty of contaminant mineralization and dye removal from wastewater. Therefore, an effective DBD reactor that can generate the plasma required for dye decomposition and mineralization removal is required. Owing to its high energy efficiency, DBD plasma has attracted considerable attention for the treatment of air pollutants [19]. Flat DBD and diffuser DBD have large discharge areas and thus allow for rapid cooling, which can create a uniform electric field. If the area is small, an arc is generated elsewhere in the frame and the electric field may be concentrated in one area. This improvement results in the production of large amounts of ozone. Additionally, the space between the discharge electrodes is narrow; therefore, these processes consume less energy, maintain high energy density, and generate high-energy and plasma active species; thus, they present several advantages [20,21]. In the application of DBD in industrial environments, its use has been for odor removal rather than dye removal [22].

In this paper, we proposed the development of a DBD plasma module that can be used at industrial sites to treat wastewater and dye-containing wastewater and increase the treatment energy efficiency. A bubbler was used to improve the interaction between the reactive species from the plasma and the dye in water, and additional active species were formed when ozone passed through the porous square tube [23–25]. Additionally, a comparative experiment was conducted using different DBDs. A 15 L reactor was manufactured and tested under the same conditions. A bubbler was fitted with a reactor of 15 L volume and the reactive bubbles from the bubbler degraded the dye in the water. The dye solution was prepared by mixing 7 L water with 1 g of MB. The performance of the flat DBD and diffuser DBD devices was evaluated under the same conditions, and the effects of the ozone concentration, dye concentration change, and energy consumption efficiency associated with the initial air flow rate were investigated. Developing a highly efficient DBD device that can be applied to industrial sites can provide advantages in terms of the cost, labor, and time.

2. Materials and Methods

2.1. Configuration of the DBD Plasma Module

Figure 1 shows a diagram of the DBD reactor. The power supply in this system used a high-voltage power supply (PCB) with a capacity of 80–140 W in power, a 19–20 kHz frequency range, a 20–80 mA current, and a transformer (UY-20) (NT Electronics, Seoul, Republic of Korea). The reactor used in this study had a rectangular shape (0.2 m × 0.15 m × 0.5 m, acrylic) and a capacity of 15 L. The experiment was conducted at a capacity of 7 L, and one bubbler was used. A square heat sink (0.08 m × 0.053 m × 0.035 m) was used for the high-voltage electrode and to ground the flat DBD module, and an electrode rod (Φ2 × 170 mm) was used for the diffuser DBD. Square quartz (SSOL Korea, Daejeon, Republic of Korea) was used as the dielectric material. The flat DBD module was composed of an in-block and out-block, and Bakelite (Changwoo Vacuum, Seoul, Republic of Korea) was used to support the bottom (Figure 1a). The discharge distance between the high-

voltage electrode and the ground was 2 mm. Ozone was generated by the plasma discharge by using a bubbler (0.05 m × 0.05 m × 0.1 m; average pore size, 100 µm; silicon oxide, 99.8%; Sam Heung Machinery, Gimhae, Republic of Korea) inserted into the reactor through a 16 mm one-touch fitting on the out-block. The diffuser DBD module consisted of an alumina tube, a ground electrode, and dielectric material. The discharge distance between the high-voltage electrode and the ground was set to 1 mm, and ozone was supplied into the reactor through an inserted bubbler. Figure 1b shows the discharge view of the flat DBD module; Figure 1c shows the schematic view of the diffuser DBD module. The optimum conditions for the DBD diffuser module were a flow rate of 30 L/min (20 L/min for plasma generation, 10 L/min for electrode cooling) and a power of 80 W, which produces a high concentration of ozone. The high-voltage electrode of the diffuser DBD plasma was a stainless-steel tube with a diameter of approximately 6 mm (thickness of 0.3 mm). In order to cool the high-voltage electrode, cooling air at a flow-rate of 10 L/min was introduced into the stainless-steel tube used as a high-voltage electrode. It was inserted into an alumina (Al_2O_3) tube with an inner diameter of roughly 5 mm (thickness of 0.5 mm). The cooling gas, which completed its task of cooling the high-voltage electrode, was designed to be used as a plasma-generating gas in combination with the discharge gas. In other words, the cooling gas prevented the high-voltage electrodes from overheating, ensuring stable plasma generation and uniform ozone production.

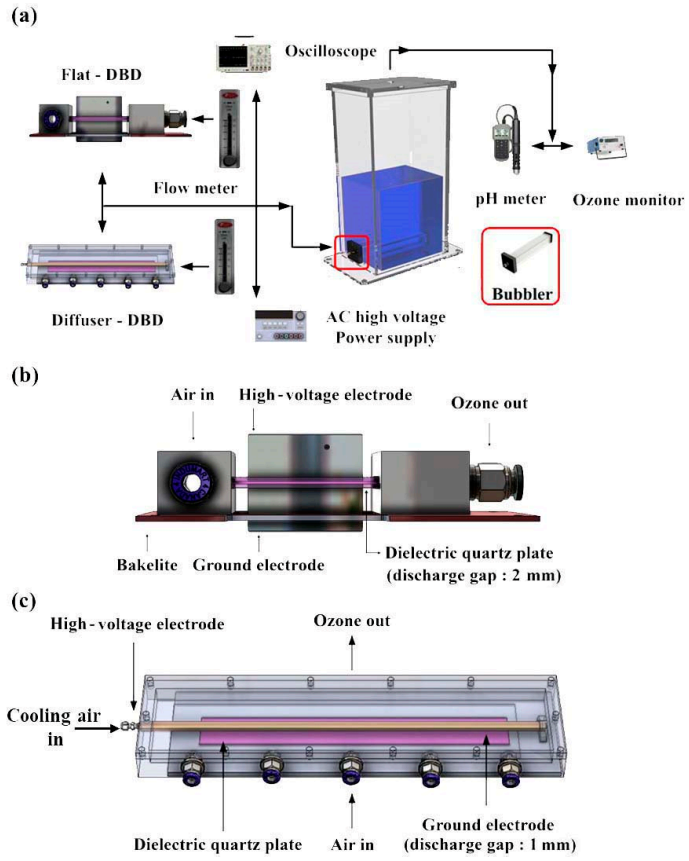

Figure 1. (**a**) Schematic of the experimental setup; (**b**) flat dielectric barrier discharge (DBD) plasma module applied to a 15 L reactor; and (**c**) diffuser DBD plasma module for methylene blue decomposition.

The plasma active species flowing into the bubbler were generated by microdischarges in the micropores on the surface and reacted directly with the MB in the reactor. This process effectively reduced the amount of dye. Additionally, the MB solution was plasma-treated for 60 min, and the decomposition rate was measured using the UV-visible absorption spectra [26–28]. The flow distribution was obtained using the COMSOL Multiphysics

program (v5.3a, Stockholm, Sweden), a commercial program for flow analysis of the bubbler in the reactor.

2.2. Analysis Equipment and Methods

Samples were collected at equal intervals of 10 min. A UV-Vis spectrometer (UV-3600; Shimadzu, Kyoto, Japan) was used to measure the degradation rate by integrating the peak of the MB. The initial concentration of MB in 7 L of water was set at 143 ppm by mixing 7 L of water with 1 g of MB (as purchased from Sigma-Aldrich, St. Louis, MO, USA, 99%). The MB degradation efficiency η was calculated as follows (5):

$$\eta\ (\%) = \frac{C_0 - C_t}{C_0} \times 100\%, \tag{5}$$

where C_0 is the initial MB concentration, and C_t is the concentration at time t.

The current and voltage were measured using a current probe (6585, Pearson Electronics, Palo Alto, CA, USA) and high-voltage probes (P6015A, Tektronix, Beaverton, OR, USA), with a digital storage oscilloscope (DPO 4054 B, Tektronix, Beaverton, OR, USA). The discharge power for the reactor was calculated as follows (6):

$$P(\mathrm{W}) = f \times \int_0^{\mathrm{T}} u(t) \cdot I(t) dt, \tag{6}$$

where W represents the discharge power, calculated by integrating the instantaneous voltage and current; f is the frequency; t is the cycle period; and $u(t)$ and $I(t)$ are oscilloscope measurements. The total power consumption was measured using a power meter (SJPM-C16, Seojun Electric, Seoul, Republic of Korea). The total power means the summation of the loss in power in the power supply and the power for plasma sustaining.

The percentage degradation of the MB dye was also defined from the absorption measurements as follows (7):

$$Decolorization\ rate(\%) = \left[1 - \left(\frac{I_t}{I_0}\right)\right] \times 100\%, \tag{7}$$

where I_0 and I_t are the absorbances of the dye without and after plasma treatment at the maximum absorption wavelength, respectively. For the MB, the absorption peak at 664 nm was within the visible range [29]. The energy yield for MB degradation can be calculated as follows (8):

$$Y\left(\frac{\mathrm{g}}{\mathrm{kwh}}\right) = \frac{C_0\left(\frac{\mathrm{g}}{\mathrm{L}}\right) \times V(\mathrm{L}) \times 0.01 \times \eta(\%)}{P(\mathrm{kW}) \times t(\mathrm{h})}, \tag{8}$$

where C and V represent the initial concentration and volume of the MB solution (1 mg/L), respectively; η is the degradation efficiency at time t; and P is the input power.

The concentration of ozone was measured at the gas outlet point of the DBD reactor by using an ozone monitor (OM-1500B, OZONETECH, Daejeon, Republic of Korea), and the measurement error was ±0.2%. The outlet ozone concentration was used to measure the ozone continuously generated from the plasma and the ozone released after sufficiently reacting with the dye. The experiment was repeated at least three times.

3. Results and Discussion

3.1. Stable DBD Generation at Atmospheric Pressure

The flat DBD plasma module showed stable discharge at 80 L/min (air) and 140 W of applied power, and the diffuser DBD module showed stable discharge at 30 L/min (air) and 80 W (Figure 1b,c) and generated high ozone concentrations. The activated species and radicals generated from the DBD module were injected into the bubbler inside the 15 L reactor. As shown in Figure 1b,c, plasma was generated inside the 2 mm (Dg) space between the insulator and electrode and the 1 mm (Dg) space between the insulator and

the electrode, respectively. The plasma remained very stable over the long-term operation periods and reacted with the MB solution to effectively decompose the dye.

3.2. Voltage and Current Waveform Analysis

The voltage and current waveforms were evaluated. As shown in Figure 2, a sharp current waveform is typically observed depending on the applied power, which is a characteristic of a typical DBD discharge [30,31]. The DBD module device was connected to the input of the power supply. For the flat DBD, the total power consumed by the power supply and plasma module at a flow rate of 80 L/min (air) was 140 W, and for the diffuser DBD, this value at a flow rate of 30 L/min (air) was 80 W. The total power is the sum of the power loss in the power supply and the power for plasma sustaining. The power supply efficiency specified by the manufacturer is approximately 80%. From Equation (6), the power applied to the two plasma modules was 112 $\pm$ 4 W for the flat DBD and 64 $\pm$ 2 W for the diffuser DBD. The small errors were due to the variation in the measurement of the discharge current. The discharge voltage of the flat DBD corresponding to the power applied to the plasma module was 3.3 kV Vrms, and the discharge current (Arms) was 42.4 mA; the discharge voltage of the diffuser DBD was 3.9 kV Vrms, and the discharge current (Arms) was 20.2 mA [32–35]. A half-cycle represents a current peak of less than a few tens of microseconds.

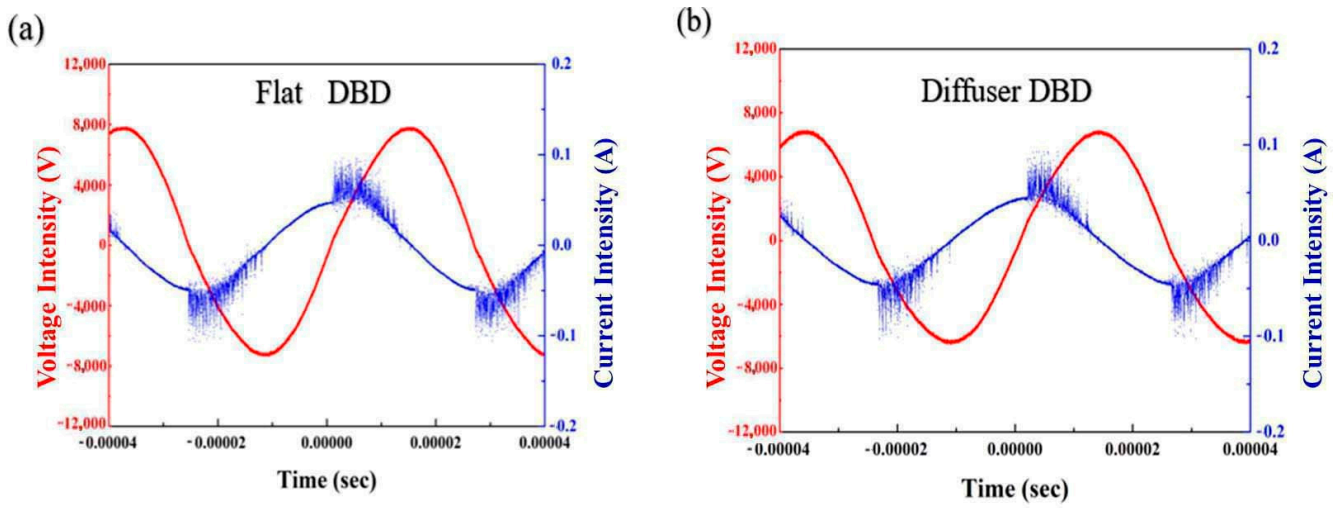

Figure 2. Voltage and current waveforms of the flat DBD and diffuser DBD at (**a**) 140 W and (**b**) 80 W total power consumption. Power consumption was calculated from the Vrms and Arms values.

3.3. Optimized Conditions from Measurements of Ozone Concentration

Figure 3 shows the graphs of the ozone concentration of the two plasma modules as a function of the input power and airflow. Ozone was generated at different input powers and air flow rates and measured at the gas outlet. We focused on a high ozone concentration and stable operation without overheating. For example, although the highest ozone concentration was measured at 80 W and 20 LPM airflow, the diffuser-type DBD overheated. In this context, we found that the optimal conditions were about 80 W at 30 LPM air and 140 W at 80 LPM for the diffuser-type DBD in Figure 3a and the flat DBD plasma module in Figure 3b, respectively. Finally, we performed the dye degradation experiments at the optimal experimental parameters using the two plasma modules and compared the degradation performances. Comparing the two plasma modules, basically, the discharge area of the flat DBD plasma module was approximately four times larger than that of the diffuser DBD plasma module, which shows that the ozone production rates of the flat DBD and diffuser DBD plasma modules were 6.5 g/h and 2 g/h, respectively. The increase in the discharge area leads more ozone production, providing more opportunities of ozone production reaction, $O_2 + O \rightarrow O_3$.

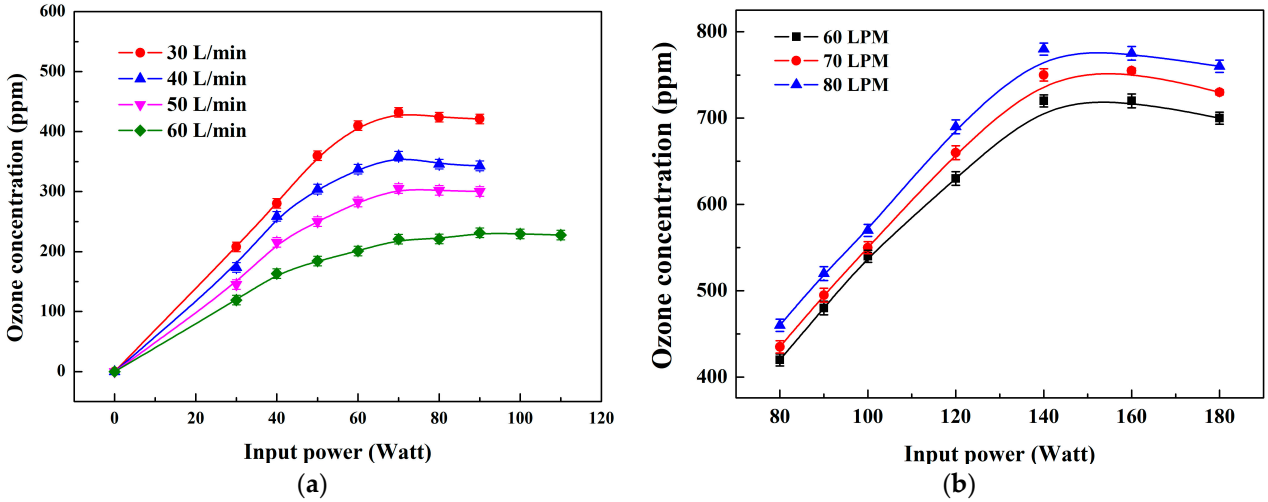

Figure 3. Graphs showing the ozone concentrations for the optimal experimental conditions of the (**a**) diffuser-type DBD and (**b**) flat DBD plasma modules. Each measurement was performed in triplicate for a given condition.

3.4. Time-Dependent Changes in Ozone Concentration during Degradation of Methylene Blue in Water

Dye degradation may require a large amount of active species during the degradation process. In this sense, the ozone concentrations were measured according to the operating time as the ozone passed through the dye in water, and these were measured at the reactor outlet. Figure 4 shows the comparison of the time-dependent changes in the ozone concentration in degrading dyes in water. The two DBD plasma modules were operated under the optimized conditions, as shown in Figure 3. The ozone gases from the plasma modules were bubbled into the liquid through a microporous bubbler inside the reactor. The initial ozone concentrations of the flat DBD and diffuser DBD plasma modules were 750 ppm and 400 ppm, respectively. As shown in Figure 4, more than 90% of the initial ozone concentration was consumed in both plasma modules, resulting in rapid degradation of the dyes in the water. After 5 min of operation, the ozone concentrations of the two plasma modules were quickly returning to the initial concentrations. The results of this experiment are consistent with the results shown in Figure 5. In this context, we observed the changes in the dye concentration over the operation time using a UV/visible spectrometer.

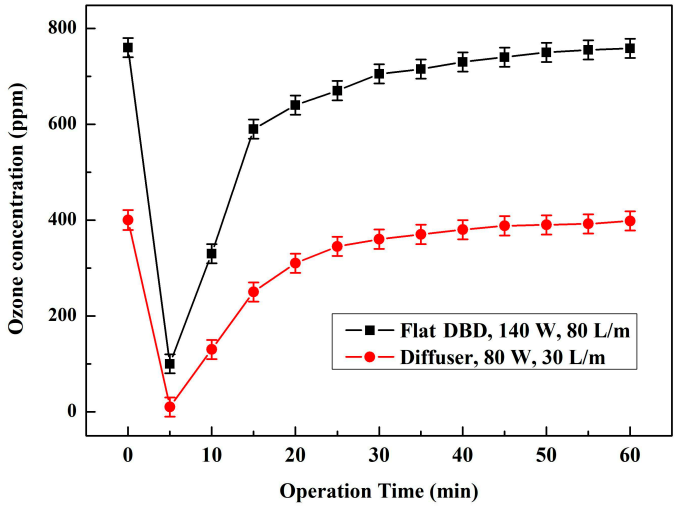

Figure 4. Comparison of the time-dependent changes in the ozone concentration in degrading dyes in water. The measured points were measured in triplicate.

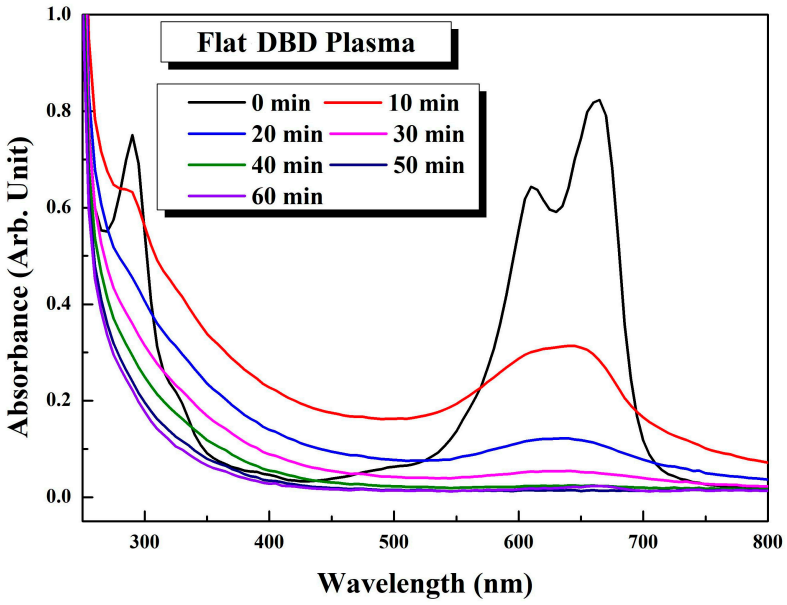

(**a**)

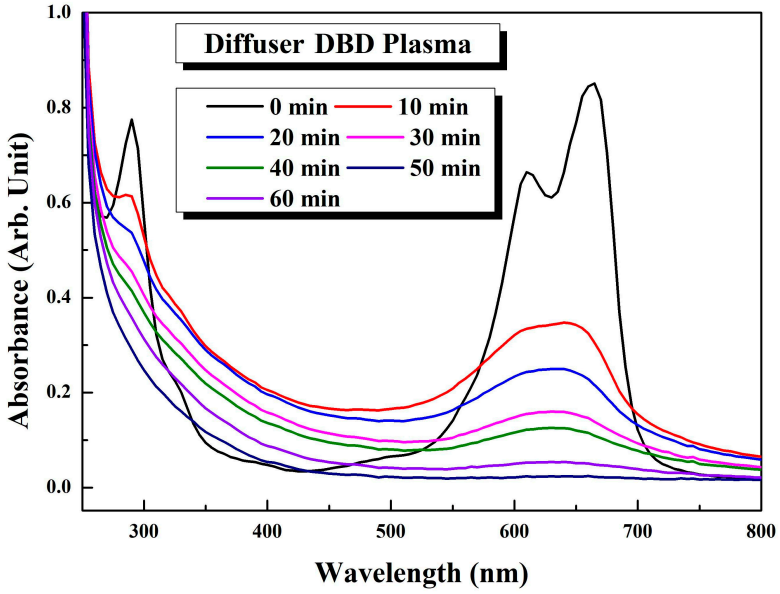

(**b**)

Figure 5. UV-visible absorbance spectra of the methylene blue solutions based on the plasma treatment time. (**a**) UV-visible absorbance spectra of the flat DBD plasma (air flow rate = 80 L/min, input power = 140 W); and (**b**) UV-visible absorbance spectra of the diffuser DBD plasma (air flow rate = 30 L/min, input power = 80 W). The initial concentration was approximately 143 ppm.

3.5. Observation of Degradation of Methylene Blue by Means of UV-Visible Spectrometer

Figure 5a,b show the UV-visible absorbance spectra of the MB degradation using the flat DBD plasma and the diffuser DBD plasma with respect to the treatment time, corresponding to the experimental conditions in Figure 4. The initial concentration of MB was set to approximately 143 ppm. The main peak of the MB near 664 nm decreased with an increasing exposure time, indicating that the dye molecules were decomposed by the plasma treatment. In the case of the flat DBD plasma, the MB was completely degraded after 40 min. On the other hand, the diffuser DBD plasma showed that the MB was completely degraded after 60 min. The difference in the degradation rate in Figure 5

results from the ozone concentration generated by the plasma modules. In this regard, we investigated the energy efficiency as a function of the specific input energy.

3.6. Methylene Blue Decomposition Efficiency

Figure 6 shows the experimental decomposition results. The analysis was conducted for 60 min at an initial MB concentration of approximately 143 mg/L, corresponding to the experimental results in Figure 5. The efficiency was low for the first 10 min but gradually increased, and complete decomposition was achieved at 40 min for the flat DBD plasma and 50 min for the diffuser DBD plasma. This was estimated using a model in water with NTP through simple primary fragmentation, The formula for the simple first-order decay model [36] is $C/C_0 = \exp(-E/\beta)$, where C represents the dye concentration remaining after the DBD treatment; C_0 represents the initial concentration; E represents the specific input energy (SIE) density during treatment; and β represents the energy density required to reduce the initial concentration to 63%. The β values of the flat DBD and the diffuser DBD plasma were 2086 J/L and 9142 J/L, respectively, explaining that the flat DBD plasma with a higher ozone concentration at a lower input energy degraded faster than the diffuser DBD plasma. Thus, the effectiveness of the flat DBD plasma treatment for MB removal was demonstrated.

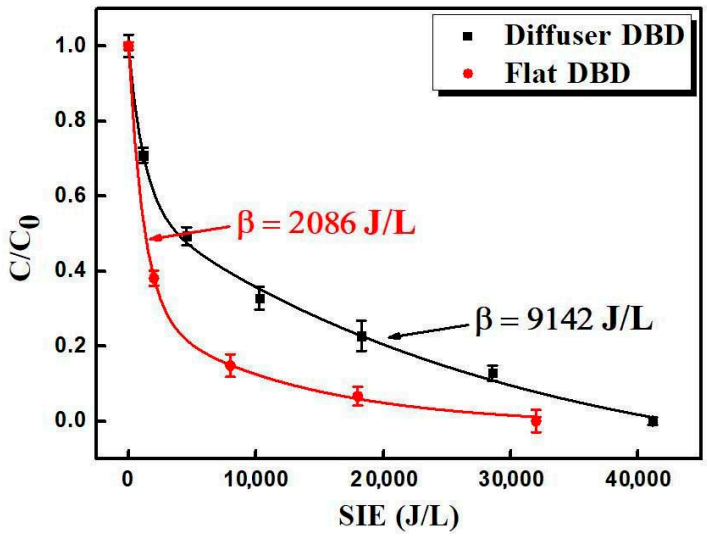

Figure 6. Effects of changes in the input energy and initial concentration of MB on the DBD process according to the input energy under optimal conditions. β represents the energy density required to reduce the concentration to 63% and SIE is the specific input energy.

In water, the half-life of ozone is much shorter than in air; in other words, ozone decomposes faster in water. When ozone is injected into water, it reacts with the water, producing hydroxyl ions and oxygen molecule from $O_3 + H_2O + 2e^- \rightarrow O_2 + 2OH^-$ [36,37]. The breakdown of MB by OH radicals leads to the formation of hydroxylated products, showing very complicated intermediate products [38]. It is beyond the scope of this paper to list all these by-products.

3.7. Mineralization of Methylene Blue

The mineralization of MB is the complete degradation of MB molecules into CO_2 and H_2O, with the total organic carbon (TOC) as an index of the degree of mineralization. In this context, Figure 7 shows the TOC analysis of the MB solution according to the treatment time. The insets are images of the MB solution with different treatment times. The TOC removal was approximately 20% after 60 min of plasma treatment. This result is higher than that obtained by Reddy et al. [39] under similar conditions. Meanwhile, the chemical oxygen demand (COD) removal reached 31% after 60 min of plasma treatment. In comparison, the

TOC removal after 30 min of ozone treatment was 14.2% [39]. This may indicate that the plasma reactor in this work can be promising for the mineralization of pollutants.

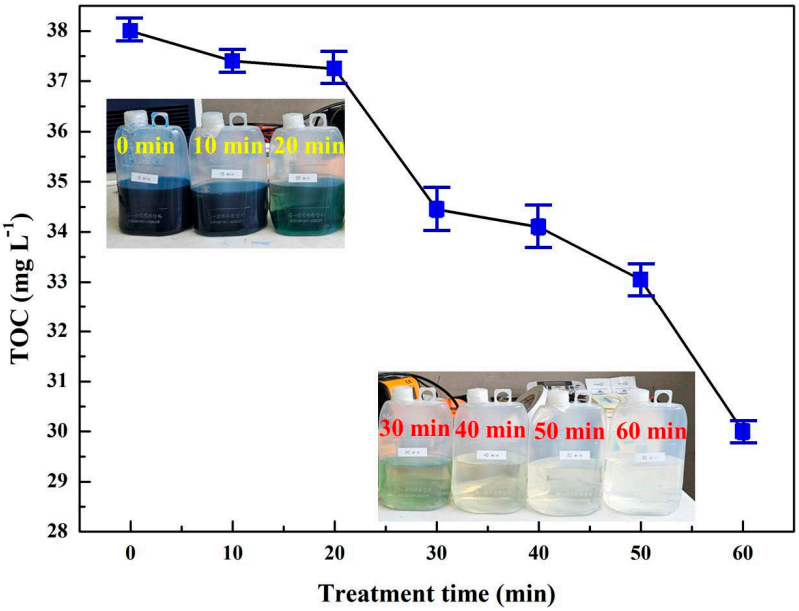

Figure 7. TOC analysis of the MB solution according to the treatment time. The insets are images of the MB solution with different treatment times.

It is widely acknowledged that OH radicals represent the most significant reactive species generated during water treatment by non-thermal plasma devices. They are capable of oxidizing the majority of organic compounds with which they come into contact in an unselective manner. Furthermore, through radical recombination, they represent the primary source of hydrogen peroxide in plasma systems. The principal methodologies entail the utilization of chemical probes that react selectively with OH radicals, thereby yielding relatively stable adducts/products that can be discerned spectroscopically (via electron paramagnetic resonance in instances where the adducts possess unpaired electrons, or through fluorimetry in cases where the adducts are fluorescent). The methods for quantifying reactive species differ depending on their half-life. In contrast to long-lived species, the concentration of OH radicals and other short-lived RS (such as superoxide, peroxynitrite, singlet oxygen, etc.) cannot be quantified by simply multiplying their formation rate by the treatment time. This is because, due to their high reactivity, they are not stable and thus do not accumulate in solution. For this reason, measuring the density of OH radicals is a further research topic. However, the concentration of hydrogen peroxide, which is a trace of the OH radical, was measured. The concentration of hydrogen peroxide was found to be 0.6 ppm at 10 min, 1 ppm at 20 min, 1.4 ppm at 30 min, and 2.3 ppm at 60 min. The applied power of the flat DBD plasma was 140 W.

3.8. Observation of the Flow Phenomenon of Bubbler Bubbles Depending on the Flow Rate

A two-phase flow was used to simulate the flow phenomenon that occurred by controlling the flow rate of the bubbles generated through a bubbler in the reactor by using the COMSOL Multiphysics program (v5.3a, Stockholm, Sweden). For the flow simulations, the governing equations are as follows. The bubbly flow interface sets up a two-stage flow model for liquid and oxygen bubbles. The physics interface covers the liquid velocity, pressure, and gas phase volume fraction. For laminar flow, the gas velocity u_g is calculated as follows: $u_g = u_1 + u_{slip}$, where u_1 represents the liquid phase velocity, and u_{slip} represents the relative velocity between gas and liquid, that is, the slip velocity. The slip speed is calculated from the slip model. We used the Hadamard–Rybczynski model, a pressure drag-balanced slip model with an adjusted drag coefficient for small spherical

bubbles. The bubble diameter is considered to be 100 µm. The laminar bubbly flow interface for this model was used to simulate the flow of liquids with dispersed bubbles. At low and moderate Reynolds numbers, the bubbles were assumed to occupy only a small volume fraction and to always move at their final velocities. Therefore, only one set of Navier–Stokes equations could be solved. For the liquid phase, we allowed the velocity of the bubbles to be guided by a slip model. Subsequently, the pressure distribution was calculated. From the average continuity equation of the mixture, the volume fraction of the bubbles was tracked by solving the effective gas density transport equation. The physical interface also determined the distribution of the number density. The interfacial area can be calculated using the number of bubbles per unit volume, which is useful for simulating chemical reactions in mixtures. The mesh was supported by software and consisted of a physics-controlled mesh. As shown in Figure 8, the flow rates were set to 30, 45, 50, 65, and 80 L/min. When the bubble flow rate was low, the wall-peaking phenomenon, in which the bubble rate was concentrated on the wall, and the core-peaking phenomenon, in which the bubble rate was high, were observed. Because air was injected into the bottom regardless of the flow rate, the air column caused was by the flow rose while shaking to the left and right. By selecting the optimal conditions through simulation and applying them to the reactor, many bubbles were able to contact the liquid surface and quickly degrade the dye agent [40]. This simulation result is consistent with the experimental results in Figures 5 and 6, which show that the flat DBD plasma with a higher ozone concentration at a higher flow rate (80 L/min) can produce more bubbles than the diffuser DBD plasma with a lower ozone concentration at a lower flow rate (30 L/min). As shown in Figure 8, as the gas flow rate increases, the bubbles occupy the inside of the reactor and create a vortex flow with rapid bubble rise. This can increase the opportunities for contact with impurities, which can rapidly degrade the MB dye.

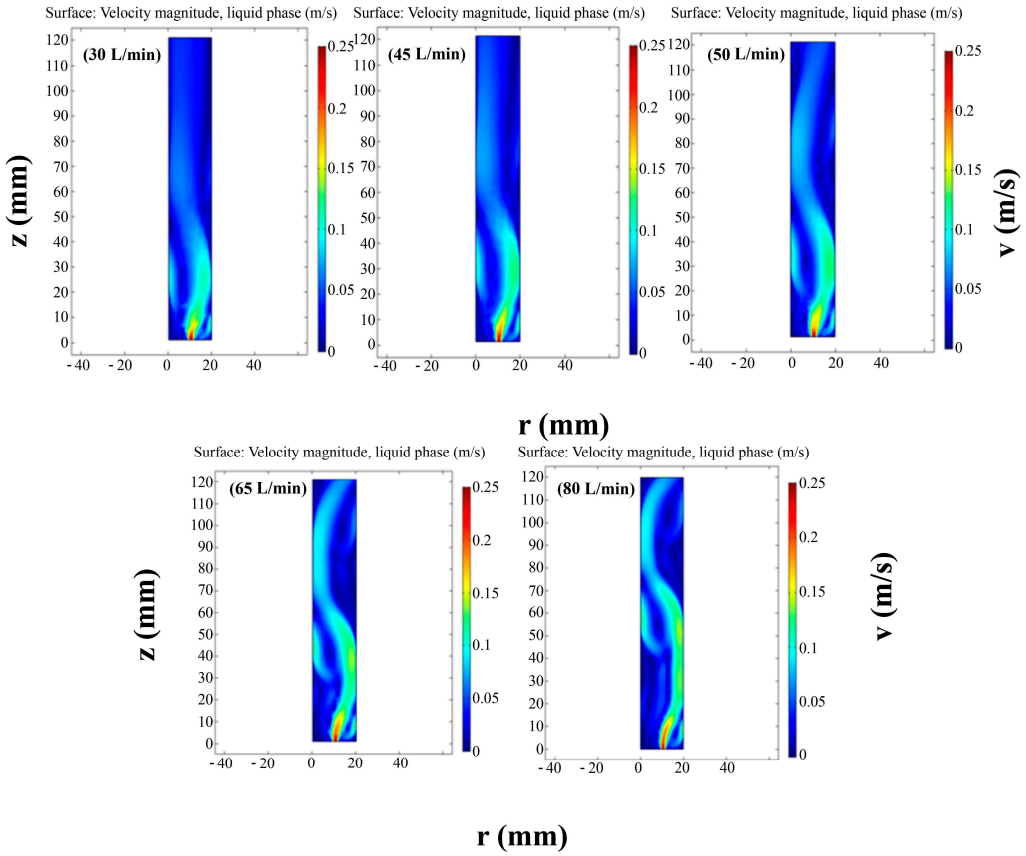

Figure 8. Contour of the instantaneous porous distribution according to the flow rates of 30, 45, 50, 65, and 80 L/min.

4. Conclusions

This study reports the use of a DBD plasma method for the decomposition of MB using NTP. We developed flat DBD and diffuser DBD devices and conducted experiments under the same conditions. The flat DBD device removed 100% of the dye in 40 min at a flow rate of 80 L/min and an output of 140 W, with an energy yield of 46.7 g/kWh and ozone production of 6.5 g/h. The diffuser DBD device completely removed the dye in 60 min at a flow rate of 30 L/min and an output of 80 W, with energy production reaching 24.6 g/kWh and ozone production reaching 2 g/h. The β values of the flat DBD and the diffuser DBD plasma were 2086 J/L and 9142 J/L, respectively, explaining that the flat DBD plasma with a higher ozone concentration at a lower input energy degraded faster than the diffuser DBD plasma. The developed NTP process brought ozone into contact with the dye through a bubbler, increasing the contact with the surface. The simulation study is consistent with the experimental results in Figures 5 and 6, which show that the flat DBD plasma with a higher ozone concentration at a higher flow rate (80 L/min) can produce more bubbles than the diffuser DBD plasma with a lower ozone concentration at a lower flow rate (30 L/min). Future studies involving enhanced plasma system structures are required to assess the treatment of water contaminants on a larger scale.

Author Contributions: Writing—original draft preparation, H.K.K.; writing—review and editing, Y.C.H.; investigation, formal analysis, data curation, G.W.Y. All authors have read and agreed to the published version of the manuscript.

Funding: This work was supported by the R&D Program under the Korea Environmental Industry & Technology Institute (KEITI) through the Aquatic Ecosystem Conservation Research Program funded by the Korea Ministry of Environment (MOE) (grant number 1485017954); the Korea Institute of Planning and Evaluation for Technology in Food, Agriculture and Forestry (IPET) and Korea Smart Farm R&D Foundation (KosFarm) through Smart Farm Innovation Technology Development Program, funded by Ministry of Agriculture, Food and Rural Affairs (MAFRA) and Ministry of Science and ICT (MISIT), Rural Development Administration (RDA) (grant number 421033-04); and the National Research Council of Science and Technology (NST) grant by the Korean Government (MSIT) (No. CAP22091-000).

Institutional Review Board Statement: Not applicable.

Informed Consent Statement: Not applicable.

Data Availability Statement: The data presented in this study are available upon request from the corresponding author. The data are not publicly available due to restrictions.

Acknowledgments: We would like to express our deepest gratitude to G&D Co., Ltd., Republic of Korea, for their help with the research and development.

Conflicts of Interest: The authors declare no conflicts of interest. The funders had no role in the study design; collection, analysis, and interpretation of data; writing of the manuscript; or decision to publish the results.

References

1. He, P.Y.; Zhang, Y.J.; Chen, H.; Liu, L.C. Development of an eco-efficient CaMoO4/electroconductive geopolymer composite for recycling silicomanganese slag and degradation of dye wastewater. *J. Clean. Prod.* **2019**, *208*, 1476–1487. [CrossRef]
2. Hanafi, M.F.; Sapawe, N. A review on the water problem associate with organic pollutants derived from phenol, methyl orange, and remazol brilliant blue dyes. *Mater. Today Proc.* **2020**, *31*, A141–A150. [CrossRef]
3. Ben Slama, H.; Bouket, A.C.; Pourhassan, Z.; Alenezi, F.N.; Silini, A.; Cherif-Silini, H.; Oszako, T.; Luptakova, L.; Golińska, P.; Belbahri, L. Diversity of synthetic dyes from textile industries, discharge impacts and treatment methods. *Appl. Sci.* **2021**, *11*, 6255. [CrossRef]
4. Berradi, M.; Hsissou, R.; Khudhair, M.; Assouag, M.; Cherkaoui, O.; El Bachiri, A.; El Harfi, A. Textile finishing dyes and their impact on aquatic environs. *Heliyon* **2019**, *5*, e02711. [CrossRef] [PubMed]
5. Roopadevi, H.; Somashekar, R.K. Assessment of the toxicity of wastewater from the textile industry to *Cyprinus carpio*. *J. Environ. Biol.* **2012**, *33*, 167–171.
6. Li, W.; Mu, B.; Yang, Y. Feasibility of industrial-scale treatment of dye wastewater via bio-adsorption technology. *Bioresour. Technol.* **2019**, *277*, 157–170. [CrossRef] [PubMed]

7. Katheresan, V.; Kansedo, J.; Lau, S.Y. Efficiency of various recent wastewater dye removal methods: A review. *J. Environ. Chem. Eng.* **2018**, *6*, 4676–4697. [CrossRef]
8. Liu, Y.; Zhang, H.; Sun, J.; Liu, J.; Shen, X.; Zhan, J.; Zhang, A.; Ognier, S.; Cavadias, S.; Li, P. Degradation of aniline in aqueous solution using non-thermal plasma generated in microbubbles. *Chem. Eng. J.* **2018**, *345*, 679–687. [CrossRef]
9. Barjasteh, A.; Dehghani, Z.; Lamichhane, P.; Kaushik, N.; Choi, E.H.; Kaushik, N.K. Recent progress in applications of non-thermal plasma for water purification, bio-sterilization, and decontamination. *Appl. Sci.* **2021**, *11*, 3372. [CrossRef]
10. Tkaczyk, A.; Mitrowska, K.; Posyniak, A. Synthetic organic dyes as contaminants of the aquatic environment and their implications for ecosystems: A review. *Sci. Total Environ.* **2020**, *717*, 137222. [CrossRef]
11. Zhang, H.; Xu, Z.; Shen, J.; Li, X.; Ding, L.; Ma, J.; Lan, Y.; Xia, W.; Cheng, C.; Sun, Q.; et al. Effects and mechanism of atmospheric-pressure dielectric barrier discharge cold plasma on lactate dehydrogenase (LDH) enzyme. *Sci. Rep.* **2015**, *5*, 10031. [CrossRef]
12. Wang, B.; Dong, B.; Xu, M.; Chi, C.; Wang, C. Degradation of methylene blue using double-chamber dielectric barrier discharge reactor under different carrier gases. *Chem. Eng. Sci.* **2017**, *168*, 90–100. [CrossRef]
13. Jiang, B.; Zheng, J.; Qiu, S.; Wu, M.; Zhang, Q.; Yan, Z.; Xue, Q. Review on electrical discharge plasma technology for wastewater remediation. *Chem. Eng. J.* **2014**, *236*, 348–368. [CrossRef]
14. Khlyustova, A.; Labay, C.; Machala, Z.; Ginebra, M.P.; Canal, C. Important parameters in plasma jets for the production of RONS in liquids for plasma medicine: A brief review. *Front. Chem. Sci. Eng.* **2019**, *13*, 238–252. [CrossRef]
15. Jodzis, S.; Barczyński, T. Ozone synthesis and decomposition in oxygen-fed pulsed DBD system: Effect of ozone concentration, power density, and residence time. *Ozone Sci. Eng.* **2019**, *41*, 69–79. [CrossRef]
16. Ainscough, T.J.; Oatley-Radcliffe, D.L.; Barron, A.R. Groundwater remediation of volatile organic compounds using nanofiltration and reverse osmosis membranes-A field study. *Membranes* **2021**, *11*, 61. [CrossRef]
17. Ksibi, M. Chemical oxidation with hydrogen peroxide for domestic wastewater treatment. *Chem. Eng. J.* **2006**, *119*, 161–165. [CrossRef]
18. Lee, H.J.; Yang, G.W.; Shin, Y.W.; Kim, K.I.; Hong, Y.C. Degradation of rhodamine b and methylene blue by underwater dielectric barrier discharge. *IEEE Trans. Plasma Sci.* **2021**, *49*, 3268–3271. [CrossRef]
19. Hong, Y.C.; Ma, S.H.; Kim, K.L.; Shin, Y.W. Multihole dielectric barrier discharge with asymmetric electrode arrangement in water and application to sterilization of aqua pathogens. *Chem. Eng. J.* **2019**, *374*, 133–143. [CrossRef]
20. Magureanu, M.; Piroi, D.; Gherendi, F.; Mandache, N.B.; Parvulescu, V.L. Decomposition of methylene blue in water by corona discharges. *Plasma Chem. Plasma Process.* **2008**, *28*, 677–688. [CrossRef]
21. Dam, T.N. Developing a decentralized wastewater treatment system using modular plasma at atmospheric pressure. In Proceedings of the 2022 6th International Conference on Green Technology and Sustainable Development (GTSD), Nha Trang City, Vietnam, 29–30 July 2022; pp. 370–374. [CrossRef]
22. Yang, G.W.; Chun, S.M.; Kim, K.I.; Lee, H.J.; Hong, Y. Simulated experiments for removal of odorous gases by wire-mesh electrode dielectric barrier discharge. *Phys. Plasmas* **2022**, *29*, 093502–093509. [CrossRef]
23. Misra, N.N.; Keener, K.M.; Bourke, P.; Cullen, P.J. Generation of in-package cold plasma and efficacy assessment using methylene blue. *Plasma Chem. Plasma Process.* **2015**, *35*, 1043–1056. [CrossRef]
24. Xiang, H.J.; Lei, B.; Yuan, X.C.; Lv, Q.A.; Zhang, Q. Design and simulation of new type reactor in the wastewater treatment system based on discharge plasma. *IEEE Trans. Plasma Sci.* **2019**, *47*, 952–957. [CrossRef]
25. Yu, S.; Chen, Q.; Liu, J.; Wang, K.; Jiang, Z.; Sun, Z.; Zhang, J.; Fang, J. Dielectric barrier structure with hollow electrodes and its recoil effect. *Appl. Phys. Lett.* **2015**, *106*, 244101. [CrossRef]
26. Hong, Y.C.; Kim, J.H.; Ma, S.H.; Cho, C.H. Volatile organic compound elimination improved on inlet position of vortex gas in microwave torch plasma. *IEEE Trans. Plasma Sci.* **2014**, *42*, 1982–1984. [CrossRef]
27. Chauhan, R.; Kumar, A.; Chaudhary, R.P. Visible-light photocatalytic degradation of methylene blue with Fe doped CdS nanoparticles. *Appl. Surf. Sci.* **2013**, *270*, 655–660. [CrossRef]
28. Ma, S.; Lee, S.; Kim, K.; Im, J.; Jeon, H. Purification of organic pollutants in cationic thiazine and azo dye solutions using plasma-based advanced oxidation process via submerged multi-hole dielectric barrier discharge. *Sep. Purif. Technol.* **2021**, *255*, 117715. [CrossRef]
29. Bansode, A.S.; More, S.E.; Siddiqui, E.A.; Satpute, S.; Ahmad, A.; Bhoraskar, S.V.; Mathe, V.L. Effective degradation of organic water pollutants by atmospheric non-thermal plasma torch and analysis of degradation process. *Chemosphere* **2017**, *167*, 396–405. [CrossRef] [PubMed]
30. Wang, C.; Zhang, G.; Wang, X.; He, X. The effect of air plasma on barrier dielectric surface in dielectric barrier discharge. *Appl. Surf. Sci.* **2010**, *257*, 1698–1702. [CrossRef]
31. Dave, H.; Ledwani, L.; Candwani, N.; Kikani, P.; Desai, B.; Chowdhuri, M.B.; Nema, S.K. Use of dielectric barrier discharge in air for surface modification of polyester substrate to confer durable wettability and enhance dye uptake with natural dye eco-alizarin. *Compos. Interfaces* **2012**, *19*, 219–229. [CrossRef]
32. Kinandana, A.W.; Yulianto, E.; Prakoso, A.D.; Faruq, A.; Qusnudin, A.; Hendra, M.; Sasmita, E.; Restiwijaya, M.; Pratiwi, S.H.; Arianto, F.; et al. The comparison of ozone production with dielectric barrier discharge plasma reactors series and parallel at atmospheric pressure. *J. Phys. Conf. Ser.* **2019**, *1217*, 012010. [CrossRef]

33. Wang, Q.; Tian, S.; Ning, P. Degradation mechanism of methylene blue in a heterogeneous Fenton-like reaction catalyzed by ferrocene. *Ind. Eng. Chem. Res.* **2014**, *53*, 643–649. [CrossRef]
34. Yang, G.W.; Lee, H.; Kim, K.; Chun, S.M.; Jeong, S.Y.; Jung, J.; Hong, Y.C. Degradation of dissolved sulfide in water using multi-hole dielectric barrier discharge. *Chemosphere* **2024**, *354*, 141687–141696. [CrossRef] [PubMed]
35. Qasim, M.; Rafique, M.S.; Naz, R. Water purification by ozone generator employing non-thermal plasma. *Mater. Chem. Phys.* **2022**, *291*, 126442–126455. [CrossRef]
36. Vo, Q.V.; Thao, L.T.T.; Manh, T.D.; Bay, M.V.; Truong-Le, B.-T.; Hoa, N.T.; Mechler, A. Reaction of methylene blue with OH radicals in the aqueous environment: Mechanism, kinetics, products and risk assessment. *RSC Adv.* **2024**, *14*, 27265–27273. [CrossRef]
37. Reddy, P.M.K.; Raju, B.R.; Karuppiah, J.; Reddy, E.L.; Subrahmanyam, C. Degradation and mineralization of methylene blue by dielectric barrier discharge non-thermal plasma reactor. *Chem. Eng. J.* **2013**, *217*, 41–47. [CrossRef]
38. Werner, J.M.; Zeng, W.; Free, M.L.; Zhang, Z.; Cho, J. Modeling and validation of local electrowinning electrode current density using two phase flow and Nernst-Planck equations. *J. Electrochem. Soc.* **2018**, *165*, E190. [CrossRef]
39. Wang, S.K.; Lee, S.J.; Jones, O.C.; Lahey, R.T. 3-D turbulence structure and phase distribution measurements in bubbly two-phase flows. *Int. J. Multiph. Flow* **1987**, *13*, 327–343. [CrossRef]
40. Hibiki, T.; Ishii, M.; Xiao, Z. Axial interfacial area transport of vertical bubbly flows. *Int. J. Heat Mass Transfer* **2001**, *44*, 1869–1888. [CrossRef]